PAPER

Wing flexibility reduces the energetic requirements of insect flight

To cite this article: Heidi E Reid et al 2019 Bioinspir. Biomim. 14 056007

View the <u>article online</u> for updates and enhancements.



IOP ebooks™

Bringing you innovative digital publishing with leading voices to create your essential collection of books in STEM research

Start exploring the collection - download the first chapter of every title for free.

Bioinspiration & Biomimetics



RECEIVED 8 February 2019

REVISED

24 June 2019

ACCEPTED FOR PUBLICATION 28 June 2019

PUBLISHED 29 July 2019

PAPER

Wing flexibility reduces the energetic requirements of insect flight

Heidi E Reid¹, Ryan K Schwab¹, Miles Maxcer², Robert K D Peterson², Erick L Johnson¹ and Mark Jankauski^{1,3}©

- ¹ Mechanical and Industrial Engineering, Montana State University, Bozeman MT, United States of America
- ² Land Resources and Environmental Sciences, Montana State University, Bozeman MT, United States of America
- ³ Author to whom correspondence should be addressed.

E-mail: mark.jankauski@montana.edu

Keywords: insect flight, flexible wings, reduced-order modeling, flight energetics, flapping wing micro air vehicles, compliant design Supplementary material for this article is available online

Abstract

Flapping insect wings deform under aerodynamic as well as inertial-elastic forces. This deformation is thought to improve power economy and reduce the energetic costs of flight. However, many flapping wing models employ rigid body simplifications or demand excessive computational power, and are consequently unable to identify the influence of flexibility on flight energetics. Here, we derive a reduced-order model capable of estimating the driving torques and corresponding power of flapping, flexible insect wings. We validate this model by actuating a tobacco hornworm hawkmoth Manduca sexta (L.) forewing with a custom single-degree-of-freedom mechanical flapper. Our model predicts measured torques and instantaneous power with reasonable accuracy. Moreover, the flexible wing model predicts experimental trends that rigid body models cannot, which suggests compliance should not be neglected when considering flight dynamics at this scale. Next, we use our model to investigate flight energetics with realistic flapping kinematics. We find that when the natural frequency of the wing is roughly three times that of the flapping frequency, flexibility can reduce energy expenditures by almost 25% compared to a rigid wing if negative work is stored as potential energy and subsequently released to do positive work. The wing itself can store about 30% of the 1200 μ J of total energy required over a wingbeat. Peak potential energy storage occurs immediately before stroke reversal. We estimate that for a moth weighing 1.5–2.5 g, the peak instantaneous power required for flight is 75-125 W kg $^{-1}$. However, these peak values are likely lower in natural insect flight, where the wing is able to exchange strain energy with the compliant thorax. Our findings highlight the importance of flexibility in flapping wing micro aerial vehicle design and suggest tuned flexibility can greatly improve vehicle efficiency.

1. Introduction

Micro air vehicles (MAVs) have become a pervasive technology over the past decade. Their applications are extensive, ranging from environmental mapping to remote sensing. Many applications require the MAV to be small so that it can navigate congested environments. For example, agricultural MAVs designed to identify stressed crops may need to negotiate dense thickets to carry out their objective effectively. However, conventional fixed-wing or rotor-based MAVs cannot be reduced to the minuscule scales necessary to carry out such tasks. At the low Reynolds numbers of small-scale flight, viscous forces dominate lift-generating aerodynamic forces and conventional rotary motors cannot dissipate heat effectively [1, 2]. Consequently, the most successful MAVs at centimeter

scale rely on flapping wings to realize flight [3]. These flapping wing micro air vehicles (FWMAVs) have the potential to revolutionize the way we carry out various tasks, including remote sensing and distributed infrastructure monitoring. Unfortunately, several issues preclude widespread realization of this promising technology. Perhaps the most obvious of these issues is inefficient energetics. Most FWMAVs demand excessive power and cannot carry their own power supplies, instead relying on tethers to provide power externally [4]. This severely limits the vehicle's autonomy and ability to perform useful tasks. By comparison, flying insects are extremely efficient, sometimes sustaining flight for several hours [5]. Thus, understanding the energetics of insect flight can guide the design and optimization of small and energy efficient robotic vehicles.

Insects are efficient fliers largely because they leverage the structural compliance of their bodies to reduce the energetic cost of flight. To flap their wings, insects deform their elastic thorax through two large sets of indirect flight muscles [6]. The small thoracic deformation is amplified into large, rotational wing motion through an intricate linkage mechanism called the wing hinge [7]. The benefit of thorax flexibility is that much of the stored strain energy can be recycled to slow down the wing upon reversal or speed up the wing at mid-stroke [8]. This diverges from a rigid system, where energy must be invested both to accelerate and to decelerate the wing. Much effort has been devoted to understand the elastic behavior of the insect thorax as well as the corresponding energy expenditures. Hollenbeck et al determined the force-displacement curve of the hawkmoth M. sexta (L.) thorax by applying varying static loads to the insects tergum [9]. Ando and Kanzaki measured the in vivo deformation of the hawkmoth A. convolvuli thorax using a high-speed laser profilometer [10]. Tu and Daniel employed a work-loop technique to actuate and measure the force and displacement of a large indirect flight muscle in an intact hawkmoth thorax [11]. Through these measurements, they were able to estimate the power requirements of flapping wing flight.

While these studies and many others focus on the flexibility and energetics of the thorax, the insect wing is a viable strain energy storage mechanism as well [12]. Like the thorax, insect wings bend and deform during flight. This deformation arises from both aerodynamic and inertial-elastic forcing [13]. Young et al used highspeed videography to measure the rotational kinematics and wing deformation of a desert locust wing [15]. They used computational fluid dynamics (CFD) to estimate the aerodynamic power for the real flexible wing and a fictitious rigid wing. Wing motion was prescribed based upon videographic measurements. They found that wing deformation reduced aerodynamic power while increasing lift. Lehmann et al studied both the aerodynamic and inertial power of flexible blow fly wings, again using high-speed videography to measure the wing deformation [16]. They conjectured spanwise bending gives rise to potential energy storage that could reduce the overall energetic cost of flight. These studies did not use predictive models to estimate wing deformation, and instead relied on experimental measurements. While this methodology is suitable for investigating specific cases of flapping wing flight, it cannot easily be extended to consider various flapping kinematics or wing designs. The ability to conduct parameter studies is essential to bio-inspired design of FWMAVS, flapping foil energy harvesters and other technologies.

To enable such parametric studies, others have developed physics-based models to estimate flapping wing energetics. Berman and Wang approximated the power-minimizing flapping kinematics of several insects in hover [17]. They assumed the wings were rigid. Stanford et al carried out a similar study for flexible wings and used an aeroelastic model to optimize the wing shape and flapping kinematics [18]. Yin and Luo studied the power economy of deformable wings and found that flexibility increases aerodynamic power efficiency [19]. In a separate study, they also showed that wing flexibility enhances thrust production during forward flight [20]. Both [19, 20] considered twodimensional motion. Nakata and Liu developed a three-dimensional high-fidelity computational fluidstructure interaction (FSI) model capable of exploring flexible wing energetics [21]. Their approach relied on a computationally intensive coupled finite element/ CFD solver. Shahzad et al utilized a coupled finite element/CFD FSI approach to study the effects of wing shape and aspect ratio on flapping wing force production and power consumption [14]. Fitzgerald et al developed a computationally efficient FSI model using an unsteady vortex lattice fluid model, though they did not consider the moments required to flap the flexible wing [22]. Quantifying the torques required to drive flexible wings is relevant to actuator sizing in insectinspired FWMAVs. Jankauski and Shen also developed a low-order model to estimate flapping wing power [12], but again this model was formulated via energy quantities and did not provide insight into the aerodynamic and inertial moments that govern power consumption. To our knowledge, there are no validated reduced-order models capable of estimating the driving torques as well as corresponding energetic expenditures of flapping wings.

Given the motivation, there are three objectives of this paper: (1) develop an accurate, low-order model capable of estimating flexible wing torques, (2) validate this model experimentally by measuring the torques of a hawkmoth wing subject to artificial flapping, and (3) estimate the energetic costs of hawkmoth flight numerically using the derived model. The model must accommodate arbitrarily complex wing geometry and be able to account for three-dimensional motion. The remainder of the paper is organized as follows. First, we derive the mathematical framework necessary to estimate the driving torques and corresponding instantaneous power of the flexible wing. We assume a simple unilaterally-coupled FSI framework, where the fluid affects the structure but the deforming structure does not affect the fluid. This assumption is reasonable for the purposes of this work because of the high mass ratio of the wings considered [14]. Next, we describe a simple single degreeof-freedom (SDOF) flapping experiment carried our to validate the mathematical model. We then compare experimental findings to numerical predictions. We conclude by investigating the energetics of a flying hawkmoth with realistic multiple degree-of-freedom (MDOF) flapping kinematics and how these energetics are affected by wing flexibility.

2. Theory

In this section, we derive a novel reduced-order method for determining the total torques and mechanical power of a flapping, flexible insect wing. We first summarize a previously developed FSI model that allows us to estimate wing deformation. We then formulate a new method to estimate the inertial torques of a flexible wing. Based upon the net torques, we calculate the total instantaneous power required to flap the wing.

2.1. Flapping wing fluid-structure interaction

The framework detailed in this section originated in [23] and [24] and is summarized here only to provide clarity to the manuscript. For a detailed derivation, the reader is encouraged to see these references. The benefit of the following FSI model is that it is reduced-order and can be solved with low computational demands. Moreover, the model is general in the sense that it can accommodate arbitrary wing geometry. Therefore, it is well-suited for high dimensional geometric or kinematic parameter studies.

First, we develop a reference frame that rotates with the rigid body motion of a wing (figure 1). A wing is placed into an inertial XYZ world-fixed coordinate. The XYZ frame undergoes a X-y''-z' rotation sequence about fixed point O with rotation amplitudes α, β and γ , respectively, where α is roll, β is pitch and γ is yaw. Note that because O is a fixed point, the motion described in this paper is representative of hovering flight. The wing-fixed xyz reference frame has an angular velocity Ω , where

$$\Omega = \underbrace{(\dot{\alpha}\cos\beta\cos\gamma + \dot{\beta}\sin\gamma)}_{\omega_x} \mathbf{e}_x + \underbrace{(\dot{\beta}\cos\gamma - \dot{\alpha}\cos\beta\sin\gamma)}_{\omega_y} \mathbf{e}_y \dots
+ \underbrace{(\dot{\gamma} + \dot{\alpha}\sin\beta)}_{\omega_z} \mathbf{e}_z.$$
(1)

Next, a position vector \mathbf{R} is drawn from fixed point O to a differential mass element in the wing-fixed frame. The position vector \mathbf{R} is

$$\mathbf{R} = \mathbf{r}_1 + W(\mathbf{r}_1, t)\mathbf{e}_z, \tag{2}$$

where \mathbf{r}_1 describes the planar coordinates of the differential mass ($\mathbf{r}_1 = x \, \mathbf{e}_x + y \, \mathbf{e}_y$) and $W(\mathbf{r}_1, t)$ is an infinitesimal, out-of-plane elastic deformation of the wing. In-plane deformation is neglected. The corresponding velocity of the differential mass is

$$\dot{\mathbf{R}} = \mathbf{\Omega} \times \mathbf{R} + \dot{W}(\mathbf{r}_1, t)\mathbf{e}_z. \tag{3}$$

We now discretize the out-of-plane deformation $W(\mathbf{r}_1, t)$ via an infinite series of space-dependent vibration mode shapes $\phi_k(\mathbf{r}_1)$ multiplied by time-dependent vibration modal responses $q_k(t)$ such that

$$W(\mathbf{r}_1, t) = \sum_{k=1}^{\infty} \phi_k(\mathbf{r}_1) q_k(t). \tag{4}$$

In the above expression, the vibration mode shapes ϕ_k can be solved either numerically via finite element analysis or experimentally via modal analysis. Vibration mode shapes are normalized with respect to the wing mass such that they satisfy orthonormal conditions. Using this discretization and the differential mass velocity (equation (3)), we formulate the kinetic energy T of the entire wing including both elastic and rigid body motion. We assume the potential energy U of the wing is described by a symmetric, quadratic strain energy density function. It follows that

$$T = \frac{1}{2} \mathbf{\Omega}^{T} \mathbf{I}_{0} \mathbf{\Omega} + \frac{1}{2} (\omega_{x}^{2} + \omega_{y}^{2}) \sum_{k=1}^{\infty} q_{k}^{2} + \frac{1}{2} \sum_{k=1}^{\infty} \dot{q}_{k}^{2} \dots$$
$$- \omega_{z} \mathbf{\Omega} \cdot \sum_{k=1}^{\infty} \mathbf{a}_{k} q_{k} - \mathbf{\Omega} \cdot \sum_{k=1}^{\infty} \mathbf{b}_{k} \dot{q}_{k}$$
$$U = \frac{1}{2} \sum_{k=1}^{\infty} \omega_{k}^{2} q_{k}^{2}. \tag{5}$$

Using the Lagrangian approach, we derive the equation of motion governing the time-dependent modal response q_k as

$$\ddot{q}_k + 2\zeta_k \omega_k \dot{q}_k + [\omega_k^2 - (\omega_x^2 + \omega_y^2)] q_k = \dot{\mathbf{\Omega}} \cdot \mathbf{b}_k - \omega_z \mathbf{\Omega} \cdot \mathbf{a}_k + Q_k,$$
(6)

where ω_k is the kth natural frequency of the wing, ζ_k is the kth viscous modal damping ratio and ω_x , ω_y are the x and y components of Ω , respectively. Note that modal damping does not arise explicitly from our derivation but is rather included after the undamped equation of motion is established. In this case, viscous modal damping may arise from both structural and fluid effects. Vectors \mathbf{a}_k and \mathbf{b}_k are directed from the fixed point of rotation O to the inertial force center of the kth vibration mode, and are defined as

$$\mathbf{a}_k = \int \phi_k(x \, \mathbf{e}_x + y \, \mathbf{e}_y) \, dm \tag{7}$$

$$\mathbf{b}_k = \int \phi_k(-y\,\mathbf{e}_x + x\,\mathbf{e}_y)\,dm. \tag{8}$$

Lastly, Q_k is the generalized aerodynamic force for the kth modal response is

$$Q_k = \int_{S} F_N(\mathbf{r}_1, t) \phi_k(\mathbf{r}_1) \, dS, \tag{9}$$

where F_N is the physical aerodynamic force normal to the wing surface S. Note that this formulation is general and F_N can be determined through any fluid modeling approach. For the purposes of this work, we use reynolds averaged Navier Stokes (RANS) CFD. Specifically, we utilize the Spalart–Allmaras RANS model with Chimera grid available to STAR-CCM + v 12.04. The Chimera meshing approach accounts for the large rigid body motion of the rotating wing without requiring remeshing of the domain.

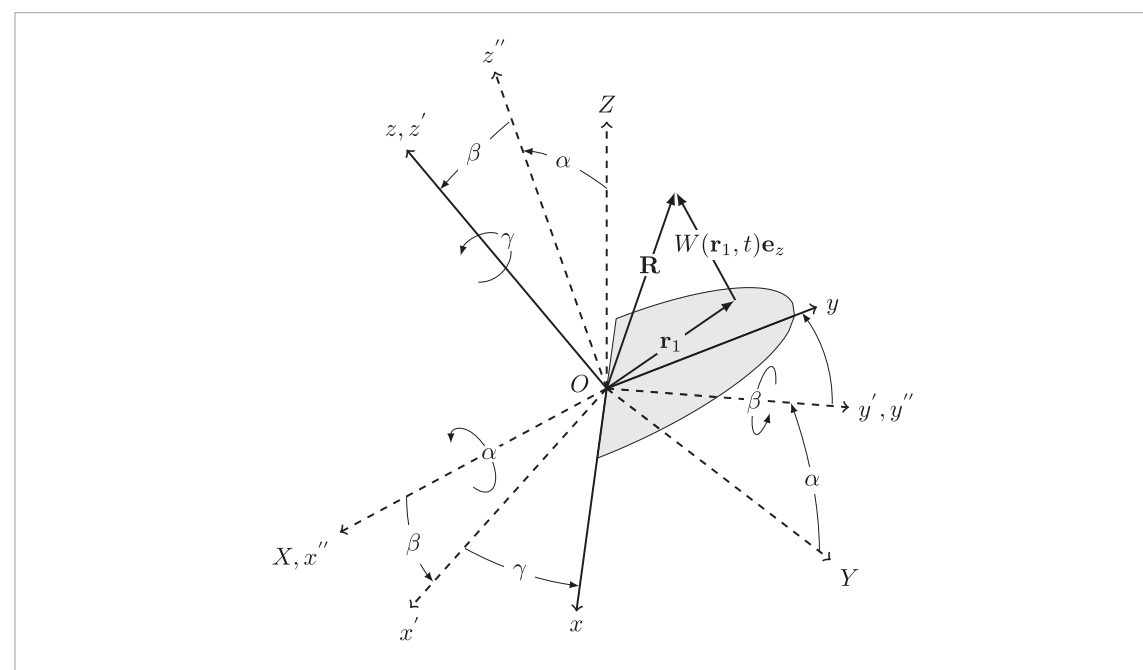


Figure 1. Rotating reference frame attached to the rigid body motion of the wing. Position vector **R** is drawn from the fixed point of origin *O* to a differential mass element.

While our model is capable of accommodating either unilateral or bilateral coupling between the fluid and structure, we assume unilateral coupling, where the flow affects the structure but the structure does not affect the flow. While this assumption is not applicable to the broad range of flapping insect wings, it is suitable for wings limited to small deformation. Moreover, it allows us to compute solutions more efficiently since CFD solvers do not need to be coupled to structural solvers. Within the context of this work, the unilateral coupling assumption yields good agreement between model and experimental predictions of moments and power. We have also observed that F_N scales quadratically with the flapping frequency and as a result can be non-dimensionalized with respect to time. Thus, a single CFD simulation can be used to identify F_N across a broad range of flapping frequencies which greatly reduces the computational resources required for this work. Other research groups have considered highfidelity bilaterally-coupled FSI models [14, 21, 25], however the lower-fidelity unliateral coupling assumption provides adequate results for the purposes of this work with low computational demands. For further detail on our CFD model, the reader is encouraged to refer to [24].

2.2. Torques and power of flexible, flapping wings

The torques of a rigid body rotating in three dimensions are well understood. However, the torques governing the rotation of a *flexible* wing are more difficult to characterize. In what follows, we derive a reduced-order method to estimate the inertial torques of a flexible wing undergoing three-dimensional rotation. In the manuscript we consider only a high-level summary of the derivation; for further detail, refer to appendix A. Since the wing rotates about a fixed point O, the angular momentum \mathbf{H}_0 about O is

$$\mathbf{H}_0 = \int_m \mathbf{R} \times \dot{\mathbf{R}} \, dm. \tag{10}$$

Substituting equations (2) and (3) into the above gives

$$\mathbf{H}_{0} = \int_{m} (\mathbf{r}_{1} + W\mathbf{e}_{z}) \times [\mathbf{\Omega} \times (\mathbf{r}_{1} + W\mathbf{e}_{z}) + \dot{W}\mathbf{e}_{z}] dm.$$
(11)

Next, out-of-plane deformation W is expanded via equation (4) which yields

$$\mathbf{H}_{0} = \sum_{k=1}^{\infty} \int_{m} (\mathbf{r}_{1} + \phi_{k} q_{k} \, \mathbf{e}_{z}) \times \left[\mathbf{\Omega} \times (\mathbf{r}_{1} + \phi_{k} q_{k} \, \mathbf{e}_{z}) + \phi_{k} \dot{q}_{k} \, \mathbf{e}_{z} \right] dm.$$
(12)

We continue to simplify the angular momentum expression until we find

$$\mathbf{H}_{0} = \mathbf{I}_{0} \mathbf{\Omega} + \sum_{k=1}^{\infty} [-q_{k}(\mathbf{a}_{k} \cdot \mathbf{\Omega})\mathbf{e}_{z} + \mathbf{b}_{k}\dot{q}_{k} \dots - (\mathbf{e}_{z} \cdot \mathbf{\Omega})\mathbf{a}_{k}q_{k} + (\mathbf{\Omega} - \omega_{z}\mathbf{e}_{z})q_{k}^{2}], \qquad (13)$$

where \mathbf{I}_0 is the wing's rigid-body inertial tensor that is constant with respect to the rotating coordinate frame. The first term to the right of the equals sign represents the rigid-body angular momentum of the wing about O. The remaining four terms are the angular momentum due to the wing's elastic deformation. The expression for \mathbf{H}_0 can be solved efficiently once the modal response q_k is calculated by equation (6). Finally, the inertial-elastic moments of the flexible wing about O are determined by differentiating \mathbf{H}_0 with respect to time such that

$$\mathbf{M}_{0.Inertial} = \mathbf{\Omega} \times \mathbf{H}_0 + \dot{\mathbf{H}}_{0,xyz},\tag{14}$$

where the first term to the right of the equals sign indicates the change in direction of the \mathbf{H}_0 and the second term indicates the change in magnitude of \mathbf{H}_0 with respect to the rotating xyz reference frame.

Lastly, the instantaneous mechanical power P(t) of the flapping wing is

$$P(t) = (\mathbf{M}_{0,Inertial} - \mathbf{M}_{0,Aero}) \cdot \mathbf{\Omega}$$
 (15)

where $\mathbf{M}_{0,Aero}$ is the aerodynamic moment determined via CFD as detailed in the previous section. This expression for total mechanical power is common in flapping wing literature. However, it is typically applied to rigid wings because an analytic expression for $M_{0,Inertial}$ for flexible structures was not previously available.

3. Experiment design

In this section, we detail an experiment intended to validate the mathematical models derived in section 2 for SDOF flapping. We first describe the fabrication of a custom mechanical flapper capable of measuring both wing driving torques and angular position. We next outline the preparation of insect specimens, as well the procedures we use to estimate insect wing natural frequencies. Finally, we discuss finite element modeling of the forewing.

3.1. Mechanical flapper

To verify the theoretical model in the previous section, we develop a simple SDOF flapper (figure 2). A video of the flapper is included in the manuscript supplementary data (stacks.iop.org/BB/14/056007/ mmedia). We equip the flapper with a custom torque load cell and optical encoder so we can directly measure the flapping torques and angular position. From these measurements, we can estimate the mechanical power required to flap the insect wing. Note that this simple experiment cannot produce the three-dimensional flapping kinematics observed in real flight. Nonetheless, it is a reasonable first attempt at validating the model derived in section 2. Then, we can use our model to estimate the torque and power requirements for flight conditions with realistic flapping kinematics. Data presented in this paper are from a single hawkmoth *M. sexta* forewing.

The central challenge of this experiment is to minimize the inertia of the flapper itself so that the torque of the wing can be clearly identified. We use a low-inertia, high-torque brushless DC motor (EC-Max16 283835, Maxon Motors) to flap the wing. The motor is equipped with an 512 count-per-turn optical encoder, which provides position feedback a combination motor controller/driver (EPOS2 24/5, Maxon Motors). The motor controller uses a PID framework to ensure that the motor shaft maintains a prescribed position profile in the presence of inertial loads. All motor commands are prescribed using Labview. The motor is bolted to a thick aluminum motor plate, and standoffs separate the motor shaft and the top aluminum plate. The top plate is equipped with a quantized 12-bit analog encoder (MAE3, US Digital) to measure the angular position of the shaft. A

slotted shaft coupler spans from the motor shaft to the analog optical encoder. During experiments, the wing is directly glued into this slot. The glue preserves the natural camber at the base of the wing.

Next, we discuss the torque measurement system. Torque measurements are challenging because insect wings have low rotational inertia. We found that due to the mass of the entire flapper, standard foil-based torque sensors were not a feasible option. Cells with the necessary low-end sensitivity were too flexible, and the reduced natural frequency of the loaded torque sensor itself interfered with the dynamic response of the wing. To mitigate this issue, we developed a custom torque transducer comprised of a piezoelectric force sensor (209C11, PCB Piezotronics) cantilevered approximately 8.9 cm from the flapper axis of rotation. The benefit to using a piezoelectric sensing element instead of a foil-based sensing element is that piezoelectric sensors are much stiffer. With this force sensor and the lever arm, the resolution of the custom torque transducer is approximately 0.008 mN m. To ensure all torque from the robotic flapper is transmitted to the load cell, we mount the entire robotic flapper on a lowfriction ball bearing.

We flap the wing at $\pm 65^{\circ}$ from 15 to 35 Hz continuously over 60 s using a swept sine. For this research we focus on measurements taken in the range of 20–30 Hz because the wing beat frequency of the M. sexta is approximately 25 Hz [26]. Measurements outside of this frequency range are used primarily to align time series data from separate trials. We perform ten trials and average the recorded torque signals from each trial. Because the overall moment of inertia of the flapping mechanism about the rotational axis is approximately 8 times larger than that of the wing, we conduct a frequency domain background subtraction to remove the influence of the flapper inertia and to identify the rotational torques of the wing only. Trials are conducted both with and without the wing, and the averaged torque measurements of the mechanism without the wing are subtracted from the averaged torque measurements with the wing. Both torque and position measurements are sampled at 2.5 kHz using a National Instruments cDAQ-9178 data acquisition system with NI 9215 analog input module.

3.2. Insect preparation

Small larvae of the tobacco hornworm, *M. sexta* (L.), were shipped overnight from Josh's Frogs (Owosso, MI) to Montana State University (MSU) and immediately placed in a rearing room (7.65 m²) with temperature of 28 °C \pm 2 °C, and a photoperiod of 24:0 (L:D) h to inhibit photoperiodic induction of pupal diapause [27]. The larvae were housed in 0.95 L insect rearing cups with perforated lids that contained Repashy Superfoods Superhorn Hornworm Gutload Diet from Repashy Ventures (Oceanside, CA). The cups were retrofitted with gutter screen to provide a structure for larvae to grasp.

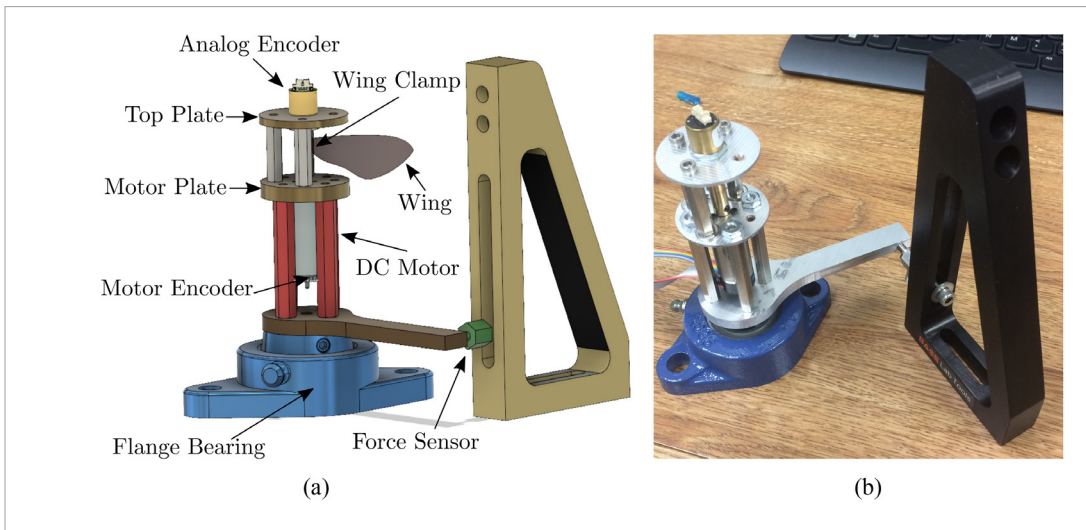


Figure 2. Computer rendering and physical realization of the SDOF mechanical flapper. The device is capable of flapping a large moth wing up to $50\,\mathrm{Hz}$ at $\pm 90\,\mathrm{degrees}$ while simultaneously measuring reaction torques and angular position of the wing. (a) Computer-drawn schematic. (b) Physical realization.

Between 3 and 6 larvae were added to each cup. Cups were inverted and organized on a rack. Following visual inspection of each larva, frass and other waste were removed daily. Larvae developed for approximately 14-21 d in these conditions. Once the aorta became prominent and the larvae ceased feeding, the larvae were transferred to a large Sterlite latching box $(23 \text{ cm L} \times 38 \text{ cm W} \times 28 \text{ cm H})$ filled uniformly with 5 cm of slightly moist peat soil. The larvae pupated within 48h in this environment. Adults emerged within 2-3 weeks of pupation and wings were allowed to fully develop before the adults were removed and sacrificed. Adult moths were sacrificed in 3.78 L glass kill jars with a plaster of Paris base and ethyl acetate killing agent. Adults were frozen immediately after euthanization and thawed in wet paper towels for 2h before experimentation. While we acknowledge freezing may affect the structural properties of the forewing, this does not preclude us from validating the derived mathematical as long as the natural frequencies of the thawed wing are quantified.

3.3. Dynamic characterization

To inform the mathematical torque model used in this research (equation (6)) we must know wing natural frequencies ω_k . This is challenging because ω_k is sensitive to boundary conditions, and the boundary condition the insect wing experiences in reality is difficult to replicate. As mentioned, the forewing is glued directly into the slotted shaft couple of the mechanical flapper to maintain the camber at the base of the wing. It is likely that the real boundary condition of the wing is more compliant and that the natural frequency is lower than what we measure experimentally. Recognizing this limitation, we explore a range of natural frequencies through simulation once the mathematical model is validated. Natural frequency data for the hawkmoth forewing is

Table 1. Parameters for finite element model of wing tested in mechanical flapper.

Parameter	Symbol	Value	Unit
Mass	m	30	mg
Surface area	A	693	mm^2
Average thickness	\bar{t}	45	$\mu\mathrm{m}$
Density	ρ	945	${\rm kg}~{\rm m}^{-3}$
Moment of inertia (x)	I_{xx}	0.163	g cm ²
Moment of iner- tia (y)	I_{yy}	0.016	g cm ²
Moment of inertia (z)	I_{zz}	0.179	g cm ²
Product of inertia (xy)	I_{xy}	0.040	g cm ²
First natural frequency	ω_1	75	Hz
Second natural frequency	ω_2	95	Hz
First Inertial Force Center	\mathbf{a}_1	$0.29 \; \mathbf{e}_x + 1.24 \; \mathbf{e}_y$	kg cm ²
Second Inertial Force Center	\mathbf{a}_2	$-0.19 \; \mathbf{e}_x - 0.21 \; \mathbf{e}_y$	kg cm ²

well documented in the literature, and the first natural frequency typically falls between 60–80 Hz [28, 29].

To identify the natural frequency of the wing mounted in the flapper, we rely on the motor to provide excitation to the wing (figure 2(a)). The motor is driven with small-amplitude broadband white noise and the output spectrum is measured at several points along the wing's surface (figure 3). We determine wing natural frequencies from single-point scans (table 1). This procedure provides noisy measurements compared to modal testing conducted with a vibration shaker, however the boundary conditions are identical to those in the flapping experiment which is critical to model validation.

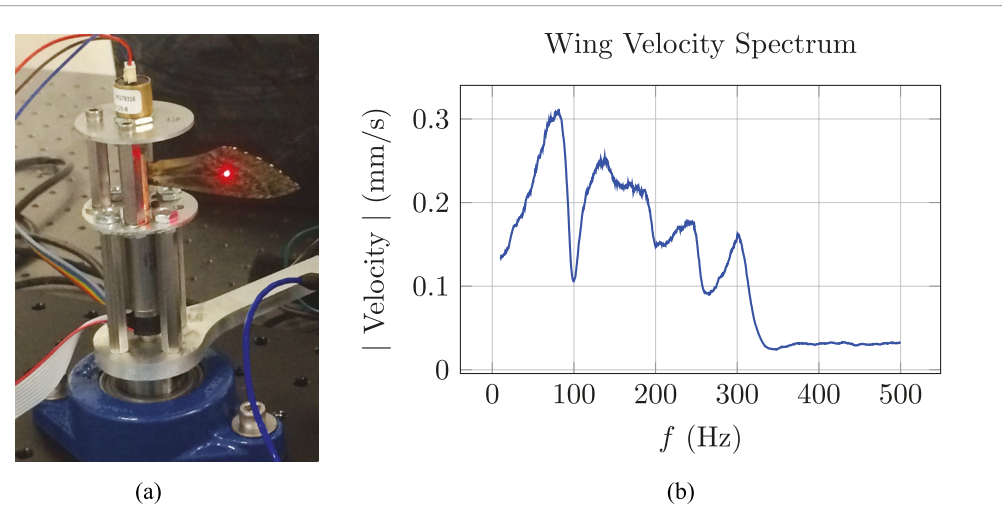


Figure 3. Measuring the natural frequency of the wing. The mechanical flapper is excited by broadband white noise with low rotational amplitude and the velocity at several points on the wing's surface is measured with the laser vibrometer. (a) Laser vibrometer measuring wing response. (b) Wing velocity output spectrum measured at a single point on wing surface with moving mean filter applied. Note that ω_2 cannot be observed from this measurement point.

3.4. Structural modeling

Lastly, we develop a simple finite element (FE) model of the insect forewing. From our FE model, we estimate mode shapes ϕ_k as well as inertial force center vectors \mathbf{a}_k and \mathbf{b}_k , which are the remaining constants required to solve the modal response equation of motion (equation (6)). Other groups have developed similar FE models [22, 28], however insect wings exhibit significant variation in morphological parameters such as surface area, mass and length [30]. Since all these parameters critically affect flapping torques and power, we must develop a FE model specific to the experimental wing rather than rely on existing FE models. We also note that while the mode shapes of our wing could be found experimentally, they will not generally satisfy the orthonormality conditions required by equation (6).

We develop our FE model using ABAQUS CAE. All model parameters are shown in table 1. We create the geometry by digitally tracing the forewing planform (figure 4). We assume constant volumetric density and vary the thickness of the wing such that the surface density agrees with existing mass distribution measurements. For more information on mass distributions, please refer to appendix B. We neglect venation and wing camber. While these assumptions do not capture the rich complexity of a real insect wing, the resulting FE model agrees reasonably well with the experimental work presented in section 4. We emphasize that the primary focus of this work is not high-fidelity FE modeling, however more complex FE models can be used with our framework if desired. For a more thorough treatment on FE modeling of insect wings, the reader is encouraged to refer to [28].

Once the FE model is created, we determine the vibration mode shapes ϕ_k and natural frequencies ω_k numerically. We find the first mode is a bending mode and the second mode is a torsional mode (figure 5)



Figure 4. Hawkmoth forewing used for the mechanical flapping experiment. FE model is based upon this wing's planform. Each grid box is $5 \, \text{mm} \times 5 \, \text{mm}$.

which agrees with past experimental modal analysis [28]. We retain only two vibration modes in this work given that higher-order modes are unlikely to be excited over the range of flapping frequencies considered. However, in other applications, high-order modes can be retained if necessary. Owing to the simplified geometric properties used in the FE model, the natural frequencies calculated numerically do not agree closely with those observed experimentally. To reconcile this, we adjust the natural frequencies of each vibration mode in post-processing so they agree with the experimental values reported in table 1. This is analogous to adjusting the directional Young's moduli

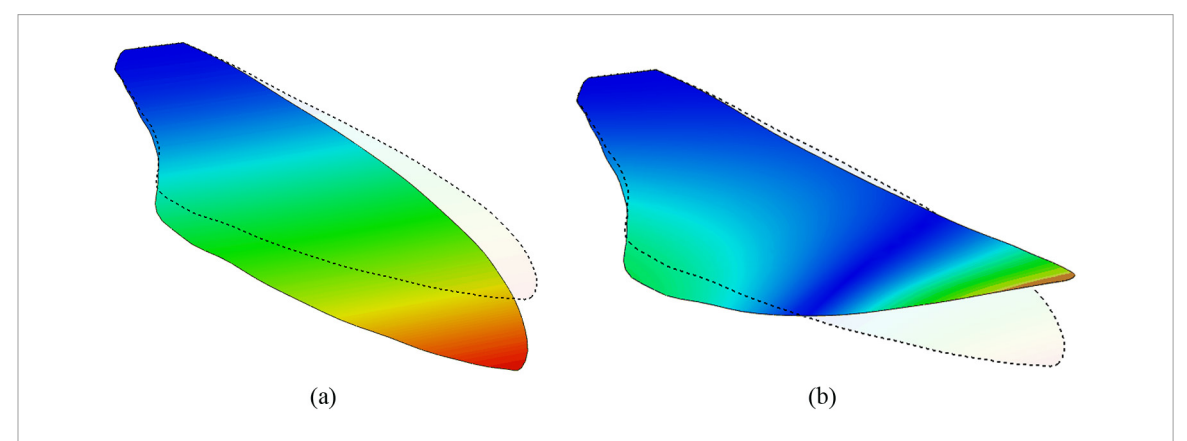
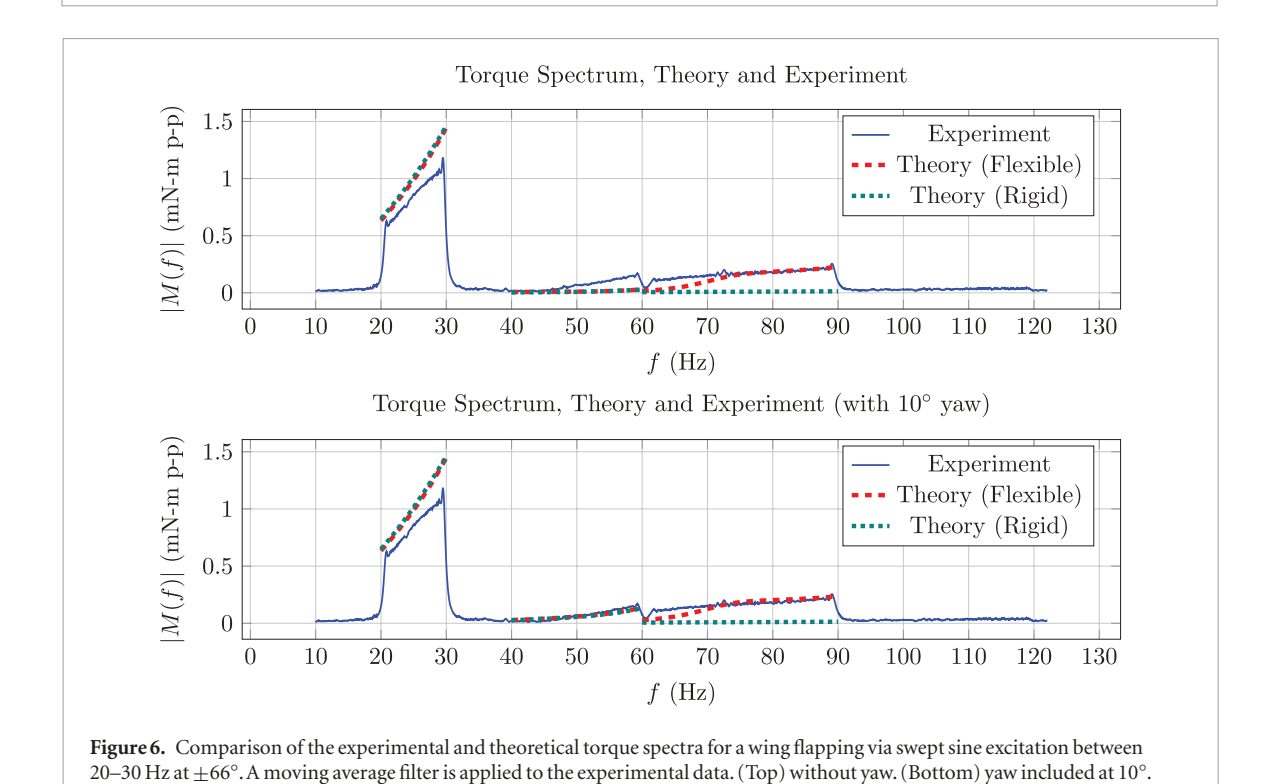


Figure 5. Vibration modes of the FE model wing superimposed on undeformed wing geometry. (a) First vibration mode (bending). (b) Second vibration mode (torsion).



so numerically predicted natural frequencies agree with those measured experimentally.

4. Results and discussion

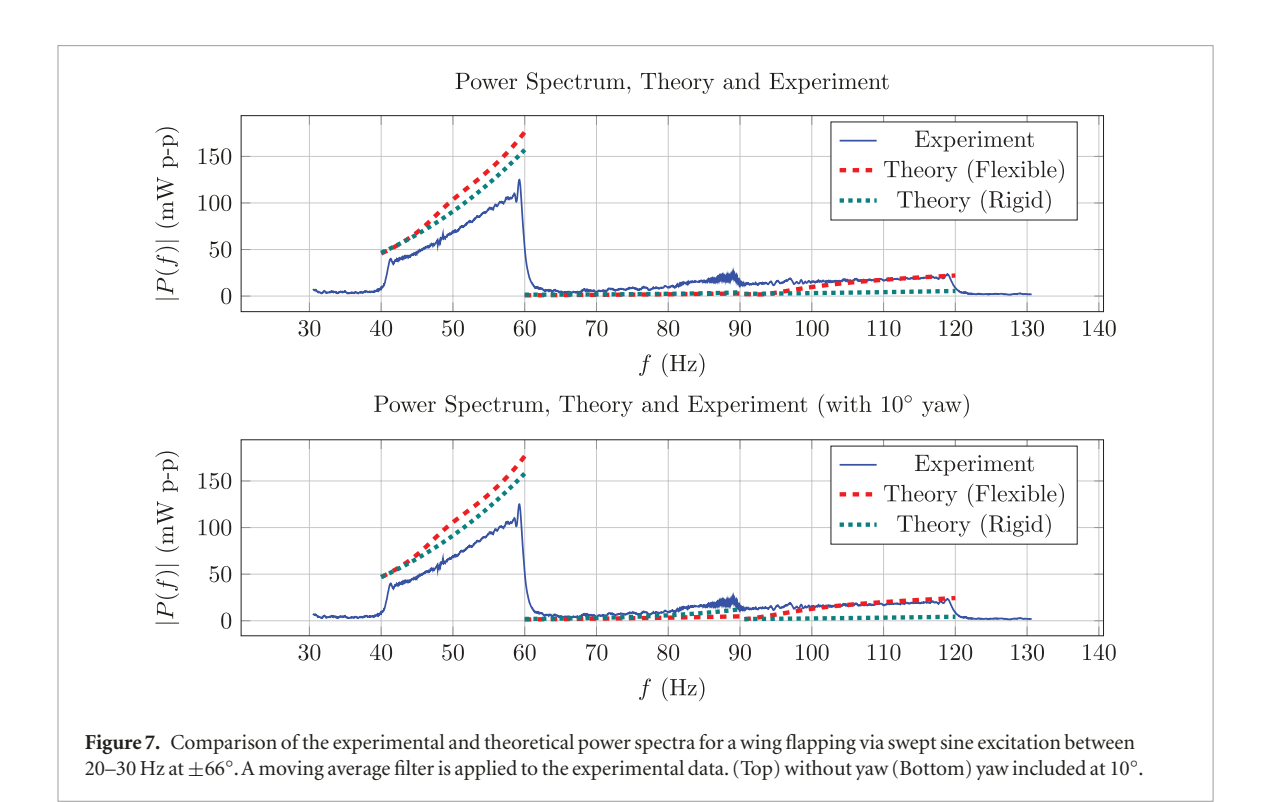
Here, we investigate the effect flexibility has on flapping wing driving torques and mechanical power. We first compare experimental data to theoretic predictions of torque and power to assess the accuracy of the mathematical model. Then, we investigate more realistic MDOF flapping kinematics via numerical simulation.

4.1. Experiment-model comparison

We first compare torque measurements taken from the 20–30 Hz swept sine flapping experiment (section 3.1) to those predicted via the mathematical model in section 2. Because swept sine simulations are computationally expensive in CFD, we instead solve

equation (6) assuming single frequency flapping and repeat this several times over the entire frequency range of interest. To attenuate the free response of the wing, we include modal damping at $\zeta = 0.1$ for both modes and simulate the numeric response over 50 wing beat periods. This damping value is selected as the average between those presented in [31] and [32] and produced good agreement between theoretical and experimental results. We record simulation data once the wing dynamics have achieved a periodic steady-state. We conduct simulations for both rigid and flexible wings to identify which model better predicts experimental trends. For each simulation with flap frequency f_{flap} , we record the magnitude of torque at f_{flap} as well as any harmonic with appreciable frequency content. The comparison between theory and experiment is shown in figure 6.

Overall, agreement between theory and experiment is good. The flexible wing theory predicts the



magnitude of flapping wing torques |M(f)| at f_{flap} and $3f_{flap}$ within reasonable accuracy. While rigid and flexible body models predict a similar torque magnitude at f_{flap} , the rigid body model cannot identify the $3f_{flap}$ response that is clearly observed in the experiment. Thus, we believe that the flexible body model more accurately predicts flapping torques and offers mathematical insights unavailable to the rigid body model.

Despite good agreement between the model and experiment, there are two discrepancies we must address. First, we see that both rigid and flexible body models slightly overstimate the torque magnitude at f_{flap} . We believe this stems from differences between the real inertial properties of the wing and those of the idealized FE model. While the cut-and-weigh procedure detailed in appendix B provides a rough estimation of the mass distribution, it is challenging to identify this distribution exactly. Even modest errors will affect the inertial properties in table 1. If the estimated moments of inertia are higher than those of the actual wing, our mathematical model will overestimate the torques at f_{flap} . Second, the experiment reveals a torque component at $2f_{flap}$ that is not accounted for by our model. This discrepancy likely comes from misalignment between the mechanical flapper and the torque sensor. If the two are misaligned by even a few degrees, the asymmetry effectively causes the wing to rotate about a secondary yaw axis. Despite being small in amplitude, the yaw rotation is geometrically coupled to the primary roll rotation and causes large gyroscopic forces to excite the wing at twice the driving frequency [23, 33]. These gyroscopic forces cause wing deformation at $2f_{flap}$ which in turn affects the torque. Indeed, if we include a yaw rotation with an amplitude of 10° into our model, it predicts the torque response at $2f_{flap}$ with excellent quantitative accuracy (figure 6, bottom).

Next, we investigate experimental energetics. We determine the instantaneous power by multiplying the measured torques with the angular velocity of the wing, where the velocity is estimated by differentiating the measured angular position. To reduce differentiation noise, we apply a low-pass filter with a 250 Hz cutoff frequency to both torque and angular velocity signals. Again, we conduct simulations to estimate the power delivered to both rigid and flexible wings and compare simulation results to experimental measurements (figure 7).

In general, the model-agreement for power magnitude |P(f)| is acceptable. The experiment shows |P(f)|occurs at $2f_{flap}$ and $4f_{flap}$ and the flexible wing model predicts the magnitude at these frequencies well. While the rigid wing theory estimates |P(f)| at $2f_{flap}$ more closely than the flexible wing theory, the rigid wing theory does not estimate any power concentrated at $4f_{flap}$. This further corroborates that the flexible wing model offers novel insight into flapping wing dynamics unavailable to conventional rigid body models. The discrepancies between the model and experiment are again due to errors in the mass distribution as well as the misalignment between the torque sensor and mechanical flapper. Reducing the inertial properties of the idealized FE wing improves the model estimates of the power magnitude at $2f_{flap}$, whereas including a small yaw rotation in the model generates a power magnitude response at $3f_{flat}$ similar to that observed in the experiment (figure 7, bottom).

4.2. Energetic costs of flight

In the previous section, we demonstrated that our model is capable of estimating the torques and power for a wing rotating about a single axis with reasonable accuracy. However, real flapping kinematics are more

Table 2. Multiple degree-of-freedom flapping kinematics.

Parameter	Description	Value	Unit
α_0	Roll amplitude	60	Degrees
β_0	Pitch amplitude	45	Degrees
γ_0	Yaw amplitude	0	Degrees
$\phi_{lphaeta}$	Pitch/roll phase difference	$\frac{\pi}{2}$	Rad
f _{flap}	Flap frequency	25	Hz

complex and wings are generally subject to multidimensional rotation. While we have yet to validate our model for MDOF rotation, we can explore the influence of wing flexibility on torques and power through numerical simulation.

First, we establish the flapping kinematics (table 2). Rotation amplitudes and phase are estimated from [26]. We include pitch and roll and neglect yaw. For simplicity, we assume all rotations are harmonic with a frequency of 25 Hz. We include modal damping at $\zeta =$ 0.05 and solve equation (6) numerically over 50 wingbeats. All results are taken from the periodic steadystate response of the wing. Because we are chiefly interested the effect of flexibility on energetics, we vary the first natural frequency of the wing ω_1 from 60 Hz to 90 Hz in 50 evenly spaced increments, conduct simulations for each natural frequency, and record net energy expended over a single wing beat. This range includes the 75 Hz natural frequency measured for the experimental wing. We maintain the second natural frequency ω_2 at 95 Hz, as we did not identify any notable changes in energetics while varying ω_2 .

According the Sun and Tang, there are two possible ways to estimate energy spent [34], which is equivalent to the work done by the driving moments. The first is to calculate the positive work done by the moment and to assume the negative work is negligible because the metabolic costs associated with negative work are small. Under this assumption, the work \mathcal{W} done is

$$\mathcal{W} = \int_0^T P^+(t) \, dt,\tag{16}$$

where T is the wing beat period and $P^+(t)$ is the positive instantaneous power. The second way to estimate energy spent is to assume negative work is stored as potential energy via some flexible structure, such as the thorax or wing itself. In this scenario, we assume that all potential energy is recovered when the wing does positive work. For this second scenario, the work done is

$$\mathcal{W} = \int_0^T (P^+(t) - |P^-(t)|) dt. \tag{17}$$

We record \mathcal{W} for both scenarios (with and without elastic storage assumed) as well as peak moments for all natural frequencies considered. We report only the moment about x, since it is significantly larger than the moments about y or z. All simulations are conducted for both rigid and flexible wings so we can identify how

the structural compliance affects moments and power. We report the ratio between quantities determined for the rigid and flexible wing (figure 8).

While flexibility tends to have a variable effect on energy expenditures, we believe structural compliance is favorable to flight efficiency. Consider the case where elastic energy storage is assumed. Across the entire range of natural frequencies, the flexible wing requires less energy to flap compared to the rigid wing. At approximately $\omega_1 = 79$ Hz, wing flexibility reduces energetic costs by as much as 25%. Interestingly, at this natural frequency, the peak moments of the flexible wing are approximately 60% higher and the peak positive power is roughly 15% higher than that required by the rigid wing. This highlights a potential tradeoff between maximum force generation and overall efficiency. These results also illuminate the importance of elastic energy storage to flight efficiency. If we assume that no elastic energy is stored and instead assume negative work is dissipated as heat, the flexible wing requires more energy to flap compared to the rigid wing. This is true over almost the entire natural frequency range considered. While some portion of energy is invariably dissipated, it is likely that a large percentage of negative work is indeed stored as potential energy and recycled over the wingbeat. Potential energy storage does not necessarily have to reside entirely in the flexible wing; instead, some percentage could be stored in the compliant thorax as well. To identify how much potential energy U is stored in the wing, we calculate the potential energy using equation (5). We evaluate the maximum potential energy U_{max} and multiply this quantity by two because potential energy storage occurs on both the wing upstroke and downstroke. We divide $2U_{max}$ by the net positive work done W^+ to identify how much energy the flexible wing can recycle relative to how much is required to flap the wing. We evaluate $2U_{max}/W^+$ over the range of natural frequencies from 60-90 Hz. The results are shown in figure 9.

The wing has the largest potential energy stored divided by energy required around $\omega_1 = 79$ Hz. At this natural frequency, the wing can store almost 30% of the energy that is required to flap the wing. We conjecture that the elastic thorax also plays a notable role in energy storage, however we cannot assess this claim because the thorax is not modeled in the present work. From this finding, we conclude that the wing itself is a viable energy storage mechanism, and one that is often overlooked in terms of robotic design. This requires that the natural frequency of the wing be tuned accordingly to achieve favorable energetics, which can be done easily via manipulation of the artificial wing geometric or material properties.

So why does $\omega_1 = 79$ Hz appear to be optimal in terms of power economy? The natural frequencies of the wing used in our experiment as well as those tested by Fitzgerald and Balachandran are close to this value [29]. Perhaps not by coincidence, this natural

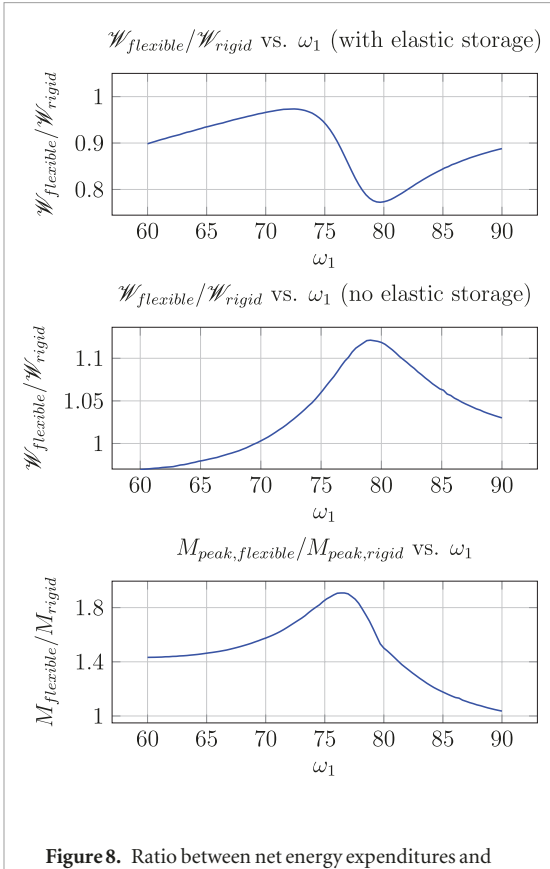


Figure 8. Ratio between net energy expenditures and peak moments for rigid and flexible wings as a function of fundamental frequency ω_1 .

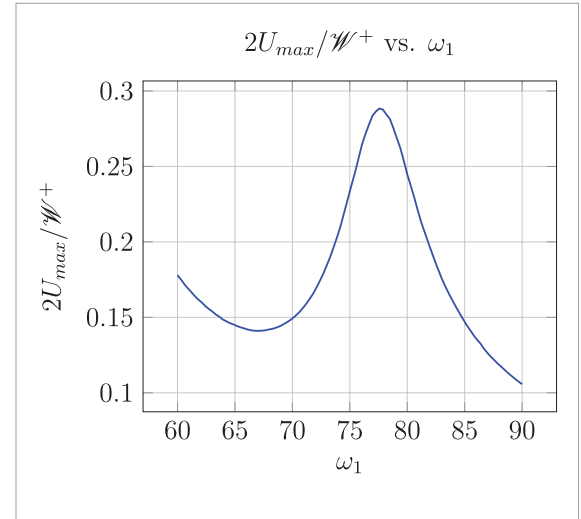


Figure 9. Ratio between the maximum potential energy storage and the energy required to flap a flexible wing as a function of the wing natural frequency.

frequency is roughly three times greater than the flapping frequency. Vanella *et al* showed via computational simulation that if an insect flaps at 1/3 its wing's natural frequency, it generates a higher lift per unit power relative to a rigid wing [35]. Dai *et al* estimated similar aerodynamic benefits for the same flapping-to-natural frequency ratio [29, 36]. Jankauski *et al* suggested that flapping at 1/3 the wing's natural frequency improves inertial power economy as well [12].

Interestingly, this flapping-to-natural frequency relationship appears across many species of flying insects [37]. We believe these aerodynamic and energetic benefits are brought about due to a near resonant response of the wing. Because the equation of motion (equation (6)) governing wing deformation is time-varying, even SDOF flapping at $\omega_{\it flap}$ will generate wing deformation at odd harmonics of ω_{flap} . If the third harmonic of the flapping frequency is near the wing fundamental frequency, the result will be a large dynamic response of the wing at three times the driving frequency. To investigate the effect of structural compliance at $\omega_1 = 79$ Hz more closely, we plot the instantaneous power for rigid and flexible wings over a wing beat in figure 10. For the flexible wing, we also plot the potential energy stored in the wing.

There are a number of interesting insights that can be determined from figure 10. We observe that for the flexible wing, the minima of negative power correspond to the maxima of potential energy. This provides further evidence that the wing serves as an energy storage mechanism. Maximum potential energy of about 160 μ J occurs immediately before the wing reversal, where the wing is transitioning from downstroke to upstroke or visa versa. It is plausible that the wing elasticity facilitates this reversal. The total energy required by the flexible wing over a wingbeat is 1200 μ J, however we emphasize that this number does not include recovered potential energy. The power delivered to the rigid wing also has a negative component, however the wing itself cannot absorb this as strain energy. Potential energy storage for the rigid wing must occur in the insect thorax or another compliant component. Nonetheless, the negative power of the rigid wing is smaller in magnitude compared to the flexible wing. This indicates that the capacity to store strain energy even in another flexible component is less than that of the flexible wing.

In terms of power, the maximum positive power is about 58 mW for the rigid wing and 95 mW for the flexible wing. Assuming the insect weighs between 1.5–2.5 g and two wings are flapping symmetrically, the mass normalized peak power is between 46–77 W kg⁻¹ for the rigid wing and 75–125 W kg⁻¹ for the flexible wing. Both rigid and flexible peak power values are on the same order of magnitude as those estimated by Daniel and Tu, who determined peak power requirements of the hawkmoth using an experimental work loop technique [11]. These values also agree with those determined by Berman and Wang, who investigated peak power requirements of a rigid hawkmoth wing computationally [17]. Thus, we feel confident our model is producing accurate quantitative results.

However, we should point out that these peak power estimates are likely greater than the real peak power required during flight. Two limitations of the present study are that (1) rotational kinematics of the wing are prescribed and (2) the wing cannot interact

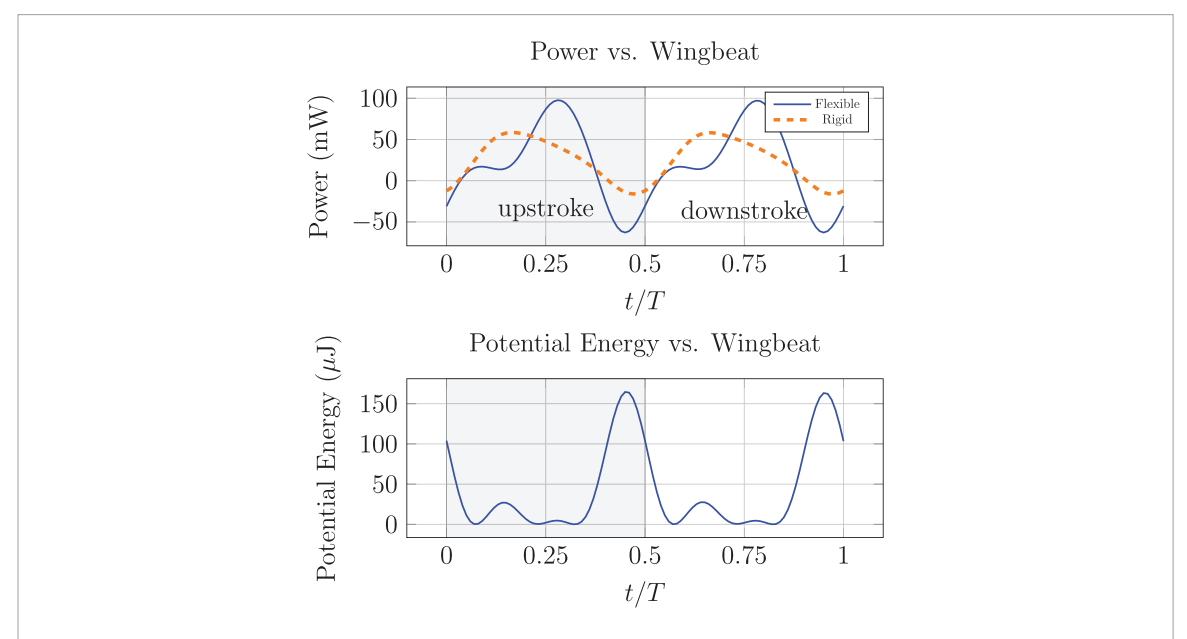


Figure 10. Power and *x*-axis moments for a rigid wing and a flexible wing with a natural frequency of $\omega_1 = 79$ Hz. Potential energy is shown for the flexible wing. The shaded gray background indicates the wing upstroke and the white background indicates the wing downstroke.

with the flexible thorax. In reality, the deformation of the wing potentially affects the deformation of the thorax, which in turn alters the rotational kinematics of the wing. The change in kinematics, and the release of potential energy stored in the thorax, may reduce the peak positive power for both rigid and flexible wings. Thus, the coupled nature of the wing-thorax must be modeled to fully realize the benefits of structural compliance on energetic efficiency. We also note that the present work does not account for aerodynamic efficiencies gained due to the wing deformation because we have assumed unilateral coupling between the fluid structure. Nonetheless, the methodology developed through this work suggests that the wing is a viable energy storage mechanism that may reduce the overall energetic cost of flight. It is probable that the flexible wing works synergistically with the elastic thorax on the system level to improve flight power economy.

The findings detailed in this section suggest that wing compliance can reduce energetic expenditures in smal, artificial flapping wing robotic vehicles. Our results suggest that the vehicle should flap at a frequency roughly 1/3 of the wing's natural frequency. This can be achieved through several simple design modifications, for example varying the wing's thickness or material. Many artificial flapping wings use small carbon fiber struts to provide support [4, 38], similar to how veins provide structural support in insect wings. Small variations in the effective diameter of these struts will substantially affect the wing's natural frequency-this is akin to how the natural frequency of a simply supported beam scales with the square value of its effective diameter [39]. Once the $\omega_{flap}/\omega_1 = 3$ ratio has been achieved via careful design, the wing will nearly resonate while flapping. As a result of the resonant response, the wing will store significant

potential energy immediately before the stroke reversal phase. Our results also indicate that the vehicles airframe or actuator system should also be compliant and capable of storing strain energy to maximize the energetic efficiency of flight.

5. Conclusions

Flapping insect wings bend and deform during flight due to the influence of both aerodynamic and inertial elastic forces. This deformation gives rise to strain energy that can potentially be recycled over a wingbeat to reduce the net energy expenditures. However, many models of flapping wing dynamics employ rigid body approximations and cannot estimate the power required by flexible wings. Many models are too high order to effectively carry out parametric studies efficiently, where the ability to conduct parametric studies efficiently is critical to bio-inspired design of FWMAVs and other technologies.

To investigate the influence of flexibility on flapping wing energetics, we develop a reduced-order model capable of estimating the torques driving a compliant wing in three-dimensional rotation. We calculate the power by taking the inner product of the torque and the angular velocity. First, we fabricate a custom SDOF flapping mechanism and use it to flap a real hawkmoth forewing. We record the torques required to flap the wing and compare those to model predictions. Overall, the agreement between model and theory for flapping wing torque and power is good. Our model predicts that flexible wings have a torque response at the flapping frequency and three times the flapping frequency whereas rigid wings have only a torque response at the flapping frequency. Experimental measurements of flexible wing torques clearly show a response at three

times the driving frequency, which shows that certain dynamic features are not well predicted by rigid body models. The derived theory also predicts experimental power trends fairly well, and again captures higherorder harmonics of instantaneous power not predicted by rigid body models.

After showing that our model works well for SDOF flapping, we explore the energetics of more realistic MDOF flapping computationally. First, we investigate the net energy spent over a wingbeat as a function of fundamental frequency ω_1 . We find that if all negative work is stored as potential energy, a flexible wing requires only 75% of the energy to flap compared to a rigid wing if the natural frequency of the flexible wing is approximately 79 Hz. However, the x-axis moment required to flap the flexible wing when $\omega_1 = 79$ Hz are 60% larger than those required to flap the rigid wing. This highlights a potential trade-off, where the flexible wing needs larger forces to generate motion but consumes less energy than the rigid wing. We estimate that the flexible wing can store approximately 30% of the total energy required over a flapping cycle.

However, to fully examine the energetic benefits of structural compliance, we recognize a need to also include the insect thorax in future modeling efforts. This will enable the wing to exchange energy with the thorax which may potentially affect the flapping kinematics. Moving forward, we will develop a general system-level model of the wing-thorax assembly that is applicable to flying insects as well as FWMAVs so we can investigate trends in system-level power flow.

Acknowledgments

This research was supported by Montana State University Norm Asbjornson College of Engineering as well as the Montana State University College of Agriculture and the Montana Agricultural Experiment Station. This material is based upon work supported by the National Science Foundation under Grant No. CBET-1855383. Any opinions, findings, and conclusions or recommendations expressed in this material are those of the author(s) and do not necessarily reflect the views of the National Science Foundation. The authors declare no conflict of interest regarding the publication of this article. We would like to thank Dr Jonathan Realmuto for his invaluable insight on methods used to evaluate energy consumption.

Appendix A. Moments of a flexible rotating structure

Here, we provide a detailed derivation of the inertial moments governing the rotation of an elastic planar wing (equation (14)). We derive these moments starting from angular momentum. Given that the rotation of the wing occurs about fixed point O, the angular momentum \mathbf{H}_0 can be written as

$$\mathbf{H}_0 = \int_m \mathbf{R} \times \dot{\mathbf{R}} \, dm \tag{A.1}$$

$$\mathbf{H}_{0} = \int_{m} (\mathbf{r}_{1} + W\mathbf{e}_{z}) \times [\mathbf{\Omega} \times (\mathbf{r}_{1} + W\mathbf{e}_{z}) + \dot{W}\mathbf{e}_{z}] dm.$$
(A.2)

For ease of derivation, we will break the angular momentum up into six terms such that

$$\mathbf{H}_{O} = \sum_{i=1}^{6} \mathbf{H}_{i}. \tag{A.3}$$

The terms, and their expansion to useful form, are detailed as follows. The first term corresponds to rigid body angular momentum and is

$$\mathbf{H}_1 = \int_m \mathbf{r}_1 \times (\mathbf{\Omega} \times \mathbf{r}_1) \, dm = \mathbf{I}_0 \mathbf{\Omega} \iff (A.4)$$

where \mathbf{I}_0 is the inertial tensor if the wing were rigid. It is constant with respect to the rotating frame. Also, due to the planar wing, $I_{xz} = I_{yz} = 0$, and $I_{xx} + I_{yy} = I_{zz}$. The remaining terms correspond to the angular momentum associated with the out-of-plane elastic deformation. We expand these terms as

$$\mathbf{H}_{2} = \int_{m} \mathbf{r}_{1} \times (\mathbf{\Omega} \times W \mathbf{e}_{z}) \, dm = \int_{m} W \, \mathbf{r}_{1} \times (\mathbf{\Omega} \times \mathbf{e}_{z}) \, dm$$
(A.5)

$$\dots = \sum_{k=1}^{\infty} q_k \int_m (\phi_k \, \mathbf{r}_1) \times (\mathbf{\Omega} \times \mathbf{e}_z) \, dm \quad (A.6)$$

$$\dots = \sum_{k=1}^{\infty} q_k \left[\mathbf{a}_k \times (\mathbf{\Omega} \times \mathbf{e}_z) \right]$$
 (A.7)

$$\dots = \sum_{k=1}^{\infty} q_k \left[\mathbf{\Omega} \left(\mathbf{a}_k \cdot \mathbf{e}_z \right) - \mathbf{e}_z \left(\mathbf{a}_k \cdot \mathbf{\Omega} \right) \right] \quad (A.8)$$

$$\mathbf{H}_{2} = -\sum_{k=1}^{\infty} q_{k} (\mathbf{a}_{k} \cdot \mathbf{\Omega}) \mathbf{e}_{z} \iff (A.9)$$

$$\mathbf{H}_3 = \int_m \mathbf{r}_1 \times \dot{W} \mathbf{e}_z \, dm = \int_m (x \, \mathbf{e}_x + y \, \mathbf{e}_y) \times \dot{W} \, \mathbf{e}_z \, dm$$
(A.10)

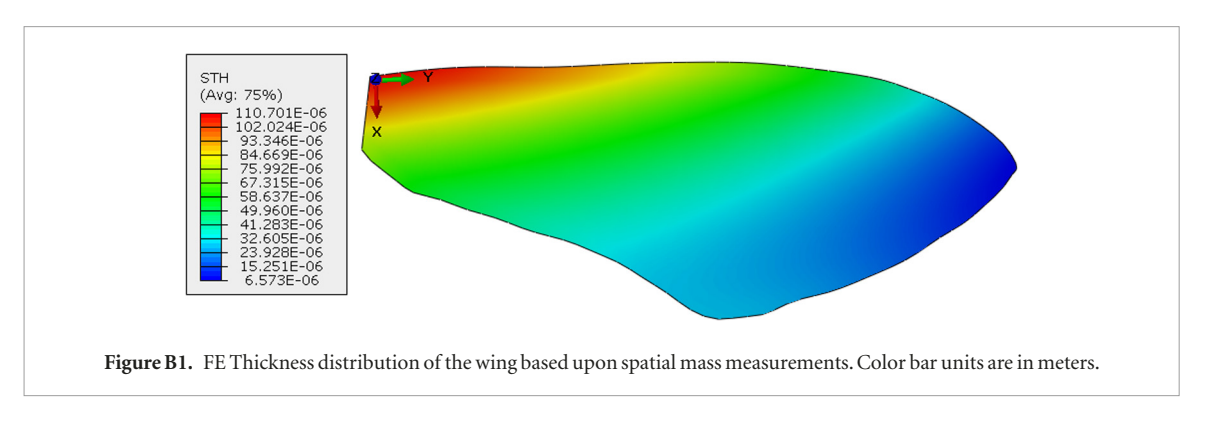
$$\dots = -\sum_{k=1}^{\infty} \dot{q}_k \int_m \phi_k(-y \, \mathbf{e}_x + x \mathbf{e}_y) \, dm \tag{A.11}$$

$$\mathbf{H}_3 = -\sum_{k=1}^{\infty} \mathbf{b}_k \, \dot{q}_k \longleftarrow \tag{A.12}$$

$$\mathbf{H}_4 = \int_m W \mathbf{e}_z \times (\mathbf{\Omega} \times \mathbf{r}_1) \, dm \tag{A.13}$$

$$\dots = \sum_{k=1}^{\infty} q_k \int_m \phi_k [\mathbf{\Omega} (\mathbf{e}_z \cdot \mathbf{r}_1) - \mathbf{r}_1 (\mathbf{e}_z \cdot \mathbf{\Omega})] dm$$
(A.14)

$$\mathbf{H}_4 = -(\mathbf{e}_z \cdot \mathbf{\Omega}) \sum_{k=1}^{\infty} \mathbf{a}_k \, q_k \iff \tag{A.15}$$



$$\mathbf{H}_5 = \int_m W \, \mathbf{e}_z \times (\mathbf{\Omega} \times W \, \mathbf{e}_z) \, dm \tag{A.16}$$

$$\dots = \sum_{k=1}^{\infty} q_k^2 \int_m \phi_k^2 [\mathbf{e}_z \times (\mathbf{\Omega} \times \mathbf{e}_z)] \, dm \tag{A.17}$$

$$\mathbf{H}_{5} = \sum_{k=1}^{\infty} q_{k}^{2} \left[\mathbf{\Omega} \left(\mathbf{e}_{z} \cdot \mathbf{e}_{z} \right) - \mathbf{e}_{z} \left(\mathbf{\Omega} \cdot \mathbf{e}_{z} \right) \right] \iff (A.18)$$

$$\mathbf{H}_6 = \int_m W \, \mathbf{e}_z \times \dot{W} \, \mathbf{e}_z \, dm = 0 \iff . \tag{A.19}$$

Lastly, we differentiate the angular momentum with respect to time, including the derivative of the rotating coordinate frame position vectors, to determine the moments acting on the wing. This gives

$$\mathbf{M}_0 = \mathbf{\Omega} \times \mathbf{H}_0 + \dot{\mathbf{H}}_0. \tag{A.20}$$

Appendix B. Wing mass distribution

In this appendix, we detail our method for estimating the mass distribution of a hawkmoth wing. The wing described hereafter is not the wing used in the flapping experiment. Instead, we assume mass distribution is similar between different wings and scale the distribution based upon the total mass.

To estimate this distribution, one left forewing from a frozen adult was thawed using a moist paper towel and a small plastic scaffold to prevent the wing coming in direct contact with the moisture. We cut the wing into 36 approximately square pieces, each approximately $5 \,\mathrm{mm} \times 5 \,\mathrm{mm}$, and the individual pieces massed on a Mettler Toledo XS205 scale accurate to 100 micrograms. We used 5 mm × 5 mm gridded paper to guide the locations of cuts made to the wing. The wing was traced and held firm to the grid during and cut with a scalpel. The wing sections were transferred from cutting surface to scale using small dissection tweezers. Each piece was placed on a piece of weighing paper and massed individually in the scale. Wing sections were then placed in order on a separate trace, covered in parafilm, and replaced in the freezer. We recorded the coordinates of each piece as well as the corresponding mass. In MATLAB, we developed

a second-order two dimensional polynomial fit of the mass distribution. We vary wing thickness while maintaining constant density to adjust the spatial surface density of the wing. The thickness variation t(x, y) is

$$t(x,y) = 0.000 1154 - 0.008 402x - 0.001 112y...$$

+ 0.1929 x^2 - 0.012 19 y^2 + 0.081 24 xy , (B.1)

where the origin is referenced from a point on the wing root (figure B1). The maximum thickness of the wing is approximately 110 μ m and the minimum thickness of the wing is approximately 6.5 μ m. The average thickness is 45 μ m, consistent with the uniform thickness used in the FE model developed by Combes and Daniel [40].

ORCID iDs

Mark Jankauski https://orcid.org/0000-0001-6305-0564

References

- Trimmer W S N 1989 Microrobots and micromechanical systems Sensors Actuators 19 267–87
- [2] Helbling E F and Wood R J 2018 A review of propulsion, power, and control architectures for insect-scale flapping-wing vehicles Appl. Mech. Rev. 70 010801
- [3] Wood R J, Finio B, Karpelson M, Ma K, Pérez-Arancibia N O, Sreetharan P S, Tanaka H and Whitney J P 2012 Progress on picoair vehicles Int. J. Robot. Res. 31 1292–302
- [4] Wood R J 2008 The first takeoff of a biologically inspired at-scale robotic insect IEEE Trans. Robot. 24 341–7
- [5] Srivastava P N and Rockstein M 1969 The utilization of trehalose during flight by the housefly, *Musca domestica J. Insect Physiol.* 15 1181–6
- [6] Dickinson M H and Tu M S 1997 The function of dipteran flight muscle *Comparative Biochem. Physiol.* A 116 223–38
- [7] Rheuben M B and Kammer A E 1987 Structure and innervation of the third axillary muscle of *Manduca* relative to its role in turning flight *J. Exp. Biol.* 131 373–402
- [8] Hollenbeck A C and Palazotto A N 2012 Methods used to evaluate the hawkmoth (Manduca sexta) as a flapping-wing micro air vehicle Int. J. Micro Air Vehicles 4 119–32
- [9] Hollenbeck A C and Palazotto A N 2013 Mechanical characterization of flight mechanism in the hawkmoth Manduca sexta Exp. Mech. 53 1189–99
- [10] Ando N and Kanzaki R 2016 Flexibility and control of thorax deformation during hawkmoth flight Biol. Lett. 12 20150733
- [11] Tu M S and Daniel T L 2004 Submaximal power output from the dorsolongitudinal flight muscles of the hawkmoth Manduca sexta J. Exp. Biol. 207 4651–62

- [12] Jankauski M, Guo Z and Shen IY 2018 The effect of structural deformation on flapping wing energetics J. Sound Vib. 429 176–92
- [13] Combes S A and Daniel T L 2003 Into thin air: contributions of aerodynamic and inertial-elastic forces to wing bending in the hawkmoth *Manduca sexta J. Exp. Biol.* 206 2999–3006
- [14] Shahzad A, Tian F-B, Young J and Lai J C 2018 Effects of flexibility on the hovering performance of flapping wings with different shapes and aspect ratios *J. Fluids Struct.* **81** 69–96
- [15] Young J, Walker S M, Bomphrey R J, Taylor G K and Thomas A L R 2009 Details of insect wing design and deformation enhance aerodynamic function and flight efficiency *Science* 325 1549–52
- [16] Lehmann F-O, Gorb S, Nasir N and Schützner P 2011 Elastic deformation and energy loss of flapping fly wings J. Exp. Biol. 214 2949–61
- [17] Berman G J and Wang Z J 2007 Energy-minimizing kinematics in hovering insect flight J. Fluid Mech. 582 153–68
- [18] Stanford B, Kurdi M, Beran P and McClung A 2012 Shape, structure, and kinematic parameterization of a power-optimal hovering wing J. Aircr. 49 1687–99
- [19] Yin B and Luo H 2010 Effect of wing inertia on hovering performance of flexible flapping wings *Phys. Fluids* **22** 111902
- [20] Tian F-B, Luo H, Song J and Lu X-Y 2013 Force production and asymmetric deformation of a flexible flapping wing in forward flight J. Fluids Struct. 36 149–61
- [21] Nakata T and Liu H 2012 A fluid-structure interaction model of insect flight with flexible wings J. Comput. Phys. 231 1822–47
- [22] Fitzgerald T, Valdez M, Vanella M, Balaras E and Balachandran B 2011 Flexible flapping systems: computational investigations into fluid-structure interactions *Aeronaut*. J. 115 593–604
- [23] Jankauski M and Shen IY 2014 Dynamic modeling of an insect wing subject to three-dimensional rotation *Int. J. Micro Air Vehicles* 6 231–51
- [24] Schwab R, Johnson E and Jankauski M 2019 A novel fluidstructure interaction framework for flapping, flexible wings (under review) *J. Vib. Acoust.*
- [25] Roccia B A, Preidikman S and Balachandran B 2017 Computational dynamics of flapping wings in hover flight: a co-simulation strategy AIAA J. 55 1806–22
- [26] Willmott A P and Ellington C P 1997 The mechanics of flight in the hawkmoth *Manduca sexta*. I. Kinematics of hovering and forward flight *J. Exp. Biol.* 200 2705–22

- [27] Bell R A, Rasul C G and Joachim F G 1975 Photoperiodic induction of the pupal diapause in the tobacco hornworm, *Manduca sexta J. Insect Physiol.* 21 1471–80
- [28] Sims T W, Palazotto A N and Norris A 2010 A structural dynamic analysis of a *Manduca sexta* forewing *Int. J. Micro Air Vehicles* 2 119–40
- [29] Fitzgerald T 2013 Nonlinear fluid-structure interactions in flapping wing systems *PhD Thesis* University of Maryland (https://doi.org/10.13016/4fsm-8q35)
- [30] Hedrick TL and Daniel TL 2006 Flight control in the hawkmoth *Manduca sexta*: the inverse problem of hovering *J. Exp. Biol.* **209** 3114–30
- [31] Eberle A L, Reinhall P G and Daniel T L 2014 Fluid-structure interaction in compliant insect wings *Bioinspiration Biomimetics* 9 025005
- [32] Norris A G 2013 Experimental characterization of the structural dynamics and aero-structural sensitivity of a hawkmoth wing toward the development of design rules for flapping-wing micro air vehicles *PhD Thesis* Air Force Institute of Technology
- [33] Jankauski M and Shen I Y 2016 Experimental studies of an inertial-elastic rotating wing in air and vacuum *Int. J. Micro Air Vehicles* 8 53–63
- [34] Sun M and Tang J 2002 Lift and power requirements of hovering flight in *Drosophila virilis J. Exp. Biol.* **205** 2413–27
- [35] Vanella M, Fitzgerald T, Preidikman S, Balaras E and Balachandran B 2009 Influence of flexibility on the aerodynamic performance of a hovering wing J. Exp. Biol. 212 95–105
- [36] Dai H, Luo H and Doyle J F 2012 Dynamic pitching of an elastic rectangular wing in hovering motion J. Fluid Mech. 693 473
- [37] San Ha N, Truong Q T, Goo N S and Park H C 2013 Relationship between wingbeat frequency and resonant frequency of the wing in insects *Bioinspiration Biomimetics* 8 046008
- [38] Ma K Y, Chirarattananon P, Fuller S B and Wood R J 2013 Controlled flight of a biologically inspired, insect-scale robot Science 340 603–7
- [39] Meirovitch L 2010 Fundamentals of Vibrations (Long Grove, IL: Waveland Press)
- [40] Combes S A and Daniel T L 2003 Flexural stiffness in insect wings II. Spatial distribution and dynamic wing bending J. Exp. Biol. 206 2989–97